

Interaction of One-Dimensional Quantum Droplets with Potential Wells and Barriers

Argha Debnath,¹ Ayan Khan,^{1,*} and Boris Malomed^{2,3}

¹*Department of Physics, School of Engineering and Applied Sciences,
Bennett University, Greater Noida, UP-201310, India*

²*Department of Physical Electronics, School of Electrical Engineering,
Faculty of Engineering, Tel Aviv University, Ramat Aviv 69978, Israel*

³*Instituto de Alta Investigación, Universidad de Tarapacá, Casilla 7D, Arica, Chile*

We address static and dynamical properties of one-dimensional (1D) quantum droplets (QDs) under the action of local potentials in the form of narrow wells and barriers. The dynamics of QDs is governed by the 1D Gross-Pitaevskii equation including the mean-field cubic repulsive term and the beyond-mean-field attractive quadratic one. In the case of the well represented by the delta-function potential, three exact stable solutions are found for localized states pinned to the well. The Thomas-Fermi approximation for the well and the adiabatic approximation for the collision of the QD with the barrier are developed too. Collisions of incident QDs with the wells and barriers are analyzed in detail by means of systematic simulations. Outcomes, such as fission of the moving QD into transmitted, reflected, and trapped fragments, are identified in relevant parameter planes. In particular, a counter-intuitive effect of partial or full rebound of the incident QD from the potential well is studied in detail and qualitatively explained.

I. INTRODUCTION

Quantum droplets (QDs) in binary Bose-Einstein condensates (BECs) originate from the interplay of the mean-field (MF) interactions and Lee-Huang-Yang (LHY) corrections to them, induced by quantum fluctuations [1]. As first demonstrated by Petrov [2], this setting is modeled by the modified Gross-Pitaevskii equation (GPE) which includes the MF self-attractive cubic term and the repulsive LHY quartic one. This prediction was followed by the creation of QDs in binary homoatomic [3–6] and heteroatomic [7] BECs, as well as in dipolar condensates [8, 9]. Actually, QDs represent a new quantum state of matter, see reviews [10, 11].

The dimensional reduction $3D \rightarrow 2D$ and $3D \rightarrow 1D$ for BEC under the action of a tight confining potential essentially changes the form of the effective GPE [12–15]. In contrast with the 3D setting, in the 1D limit the LHY term has the self-attraction sign, and is quadratic, rather than quartic [12]. However, it is also possible to extend the 3D framework to a quasi-one-dimensional (Q1D) geometry by tuning the transverse confinement suitably. In this situation, the repulsive quartic LHY term prevails to support the droplet formation in both homogeneous and inhomogeneous systems [16, 17]. Similarly, the quartic term provides stabilization of Q2D bound states pulled to the center by the singular potential $\sim -1/r^2$ [18].

On the contrary, in the proper 1D system the residual self-repulsive MF term competes with the quadratic self-attraction, making it possible to create broad QD states with the equilibrium density in their inner quasi-flat parts [19, 20]. The fact that the density cannot exceed the equilibrium value implies that the quantum matter filling the QDs is an incompressible liquid, therefore localized states are named “droplets”.

The next natural step in the studies of the droplet dynamics is to investigate collisions between moving QDs, which was realized experimentally (in the 3D geometry) in Ref. [6]. In the 1D setting, simulations of the corresponding GPE with the cubic-quadratic nonlinearity demonstrate that the collision between slowly moving droplets with zero phase difference between them leads to their merger into a single one, in an excited (breathing) state, while the collision between QDs with phase difference π ends up with quasi-elastic rebound [19]. Collisions at large velocities tend to produce quasi-elastic outcomes, i.e., passage of the QDs through each other, similar to collisions between usual matter-wave solitons [21].

Another physically relevant problem is the consideration of collisions of an incident QD with a confined attractive or repulsive defect, which may be represented by a localized potential well or barrier, respectively. In the experiment, such defects can be created, respectively, by narrow red- or blue-detuned laser beams illuminating the condensate [22]. For moving solitons this problem was considered, in various forms, in the framework of the nonlinear Schrödinger equation (NLSE) [23–30]. In BEC, collisions of matter-wave solitons with barriers were studied both theoretically [31–34] and experimentally [22]. In particular, much interest was drawn to the use of narrow potential barriers as splitters in the design of soliton interferometers [35–40]. Bound states of low-dimensional QDs interacting with defects were recently addressed in Refs. [41–43]. Removable potential barriers can be used for preparation of inputs initiating collisions between condensates [44].

In this work, we aim to study interactions of QDs with potential wells and barriers in the framework of the one-dimensional LHY-corrected GPE with the cubic-quadratic nonlinearity. The corresponding model is formulated in Sec. II. Analytical results obtained for the model are collected in Sec. III. In particular, we consider quiescent QDs trapped in potential wells. For the nar-

* ayan.khan@bennett.edu.in

row well represented by the delta-function potential we present three exact stable solutions for localized states pinned to the well. The Thomas-Fermi and adiabatic approximations are considered too, for pinned and moving QDs, respectively. Collisions of moving QDs with the barrier or well are studied by means of systematic simulations in Sec. IV. The outcome of the collisions is quantified by computing shares of the initial norm in the transmitted, reflected and trapped waves (trapping takes place in the case of the potential well). We also plot maps, in the plane of the norm and velocity of the incident QD, for values of the maximum strength of the potential well admitting full transmission, and minimum strength required for the observation of a counter-intuitive effect, in the form of the *complete reflection* of the moving QD from the attractive potential. The paper is concluded by Sec. V.

II. THE MODEL

In this section we summarize the 1D theoretical model. We start from the binary BEC with equal self-repulsion coefficients in both components, $g_{11} = g_{22} = g > 0$, and equal numbers of atoms in them. This setting makes it possible to consider the symmetric configuration, with equal MF wave functions of the components, $\psi_1 = \psi_2 \equiv \psi$. Then, defining a small difference between the inter-component attraction strength ($g_{12} < 0$) and intra-component self-repulsion, $\delta g = g + g_{12} > 0$, with $\delta g \ll g$, one can derive the effective 1D GPE including the beyond-MF correction (the quadratic term) as [12]:

$$i\hbar \frac{\partial \psi}{\partial t} = -\frac{\hbar^2}{2m} \frac{\partial^2 \psi}{\partial x^2} + f(x)\psi + \delta g |\psi|^2 \psi - \frac{\sqrt{2m}}{\pi\hbar} g^{3/2} |\psi| \psi, \quad (1)$$

where $f(x)$ represents an external potential, and m is the atomic mass.

Equation (1) determines characteristic units of length, x_0 , time, t_0 , energy, E_0 , and wave function,

$$x_0 = \frac{\pi\hbar^2\sqrt{\delta g}}{\sqrt{2m}g^{3/2}}, t_0 = \frac{\pi^2\hbar^3\delta g}{2mg^3}, \quad (2)$$

$$E_0 = \frac{\hbar^2}{mx_0^2} = \frac{\hbar}{t_0}, \psi_0 = \frac{\sqrt{2m}}{\pi\hbar\delta g} g^{3/2},$$

which suggests rescaling $t \equiv t_0\tilde{t}$, $x \equiv x_0\tilde{x}$, $\psi \equiv \psi_0\tilde{\psi}$, $f'(x) \equiv f(\tilde{x})/E_0$. In this notation, Eq. (1) is cast in the normalized form (where the tildes are omitted):

$$i\frac{\partial \psi}{\partial t} = -\frac{1}{2} \frac{\partial^2 \psi}{\partial x^2} + f(x)\psi + |\psi|^2 \psi - |\psi| \psi, \quad (3)$$

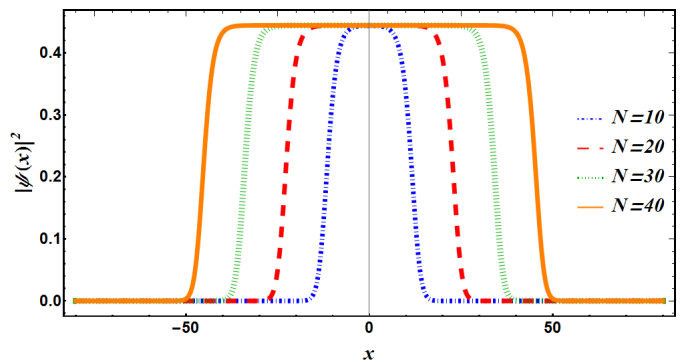


FIG. 1. (Color Online) Spatial density distributions, $|\psi(x)|^2$, as given by the QD solution in Eq.(7), for different values of norm noted in Eq.(9), as indicated in the figure.

with Hamiltonian (energy),

$$E = \int_{-\infty}^{+\infty} \left[\frac{1}{2} \left| \frac{\partial \psi}{\partial x} \right|^2 + f(x)|\psi(x)|^2 - \frac{2}{3} |\psi(x)|^3 + \frac{1}{2} |\psi(x)|^4 \right] dx \quad (4)$$

$$\equiv E_{\text{kin}} + E_{\text{int}},$$

which includes the kinetic, alias gradient (first), and interaction (potential) terms.

Stationary solutions for QDs with chemical potential $\mu < 0$, produced by Eq. (3), are looked for in the usual form,

$$\psi(x, t) = \exp(-i\mu t) \phi(x), \quad (5)$$

where real stationary wave function $\phi(x) > 0$ satisfies the equation

$$\mu\phi = -\frac{1}{2} \frac{d^2\phi}{dx^2} + f(x)\phi + \phi^3 - \phi^2. \quad (6)$$

In particular, the free-space version of Eq. (6), with $f(x) = 0$, gives rise to the known family of exact QD solutions [12],

$$\phi(x) = -\frac{3\mu}{1 + \sqrt{1 + 9\mu/2} \cosh(\sqrt{-2\mu}x)}, \quad (7)$$

where $\mu < 0$ is the chemical potential, which takes values in a finite bandgap,

$$0 < -\mu < 2/9. \quad (8)$$

The norm of the QD state can be derived from Eq.(7) such that, [12]

$$N = \int_{-\infty}^{+\infty} |\psi(x)|^2 dx = \frac{4}{3} \left[\ln \left(\frac{3\sqrt{-\mu/2} + 1}{\sqrt{1 + 9\mu/2}} \right) - 3\sqrt{-\mu/2} \right]. \quad (9)$$

Note that the dependence $N(\mu)$, as given by Eq. (9), satisfies the celebrated Vakhitov-Kokolov (VK) criterion,

$$dN/d\mu < 0, \quad (10)$$

which is a necessary condition for the stability of localized states supported by any self-attractive nonlinearity [45–47].

In the limit of $\mu \rightarrow -0$, the QD state (7) is similar to traditional solitons dominated by the quadratic nonlinearity, such as ones produced by the Korteweg – de Vries equation [48, 49],

$$\phi(x) \approx -\frac{3\mu}{2 \cosh^2(\sqrt{-\mu/2}x)}. \quad (11)$$

In the opposite limit, $\mu \rightarrow -2/9$ [see Eq. (8)], Eq. (7) produces quasi-flat droplets (“puddles”, in terms of Ref. [19]), with the nearly constant inner density,

$$\phi^2(x) \leq n_{\max} = 4/9, \quad (12)$$

and a logarithmically large width,

$$L \approx (3/2) \ln [1 / (1 + 9\mu/2)]. \quad (13)$$

Exactly at the border of the bandgap (8), $\mu = -2/9$, QD (7) carries over into the front solutions,

$$\phi_{\text{front}}(x; \mu = -2/9) = \frac{2/3}{1 + \exp(\pm 2x/3)}, \quad (14)$$

which connect the zero state and the constant-amplitude (alias continuous-wave, CW) one,

$$\psi_{\text{CW}} = (2/3) \exp((2/9)it). \quad (15)$$

In fact, the front solutions (14) represent boundaries of a very broad flat-top QD.

Density profiles of the QD solution (7) with different values of N are plotted in Fig. 1. In the figure, the profiles corresponding to $N = 20, 30$, and 40 clearly exhibit the flat-top shape. In agreement with the prediction of the VK criterion, all the QDs (7) are stable solutions of Eq. (3).

The Galilean invariance of Eq. (3) [with $f(x) = 0$] makes it possible to set the QD in motion by application of the boost (kick) to them with arbitrary parameter k , which determines the velocity of the moving mode:

$$\psi(x, t) = \exp[ikx - i(k^2/2)t] \psi(x - kt, t). \quad (16)$$

The effective mass of the moving QD coincides with its norm N , i.e., its kinetic energy is

$$E_{\text{kin}} = N(k^2/2). \quad (17)$$

This result is used below to predict the threshold of the rebound of the moving QD from a potential barrier, see Eq. (41).

III. ANALYTICAL RESULTS

A. Localized modes pinned to narrow potential wells: exact solutions

Our primary objective is to consider interactions of QDs with a potential well/barrier, as described by Eq.

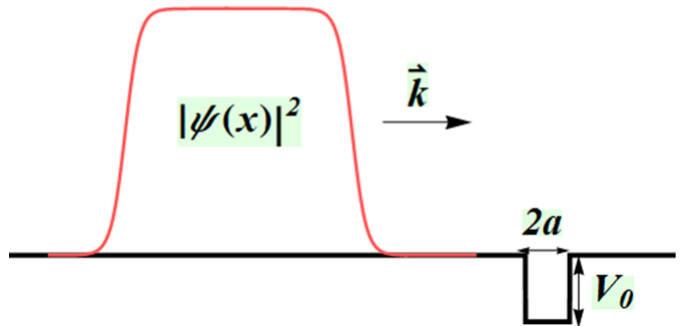


FIG. 2. (Color Online) A schematic representation of a flat-top QD colliding with a rectangular potential well with width $2a$ and depth V_0 .

(3) with $f(x) \neq 0$ and illustrated by Fig. 2. In this figure, the local potential is taken as a rectangular well of width $2a$ and depth $V_0 > 0$:

$$f(x) = \begin{cases} -V_0, & \text{for } -a < x < +a, \\ 0, & \text{for } |x| > a. \end{cases} \quad (18)$$

The same potential with $V_0 < 0$ represents a rectangular barrier of height $-V_0$.

In this section we present analytical findings which for the case when the finite well/barrier is approximated by a delta-function potential. The approximation is valid provided that the width of the potential well is much smaller than the size of the QD. In this limit, we obtain exact analytical results which are later qualitatively corroborated by our numerical study.

Hence, we assume,

$$f(x) = f_\varepsilon(x) = -\varepsilon\delta(x), \quad (19)$$

with strength

$$\varepsilon \equiv 2aV_0. \quad (20)$$

The same potential (19) with $\varepsilon < 0$, i.e., $V_0 < 0$ in Fig. 2, represents a narrow potential barrier, such as the one used as the soliton splitter in interferometers [35–39].

Exact analytical solutions for nonlinear modes pinned to the delta-function potential well defined by Eq. (19) are produced below. We substantiate these analytical results by comparison with their numerically found counterparts, as shown in Fig. 3(a,b). The respective numerical solutions of Eq. (6) were produced with the δ -potential approximated by means of the standard Gaussian,

$$\tilde{\delta}(x) = \frac{1}{\sqrt{\pi}\sigma} \exp\left(-\frac{x^2}{\sigma^2}\right), \quad (21)$$

with a small width, $\sigma = 0.03$ [50].

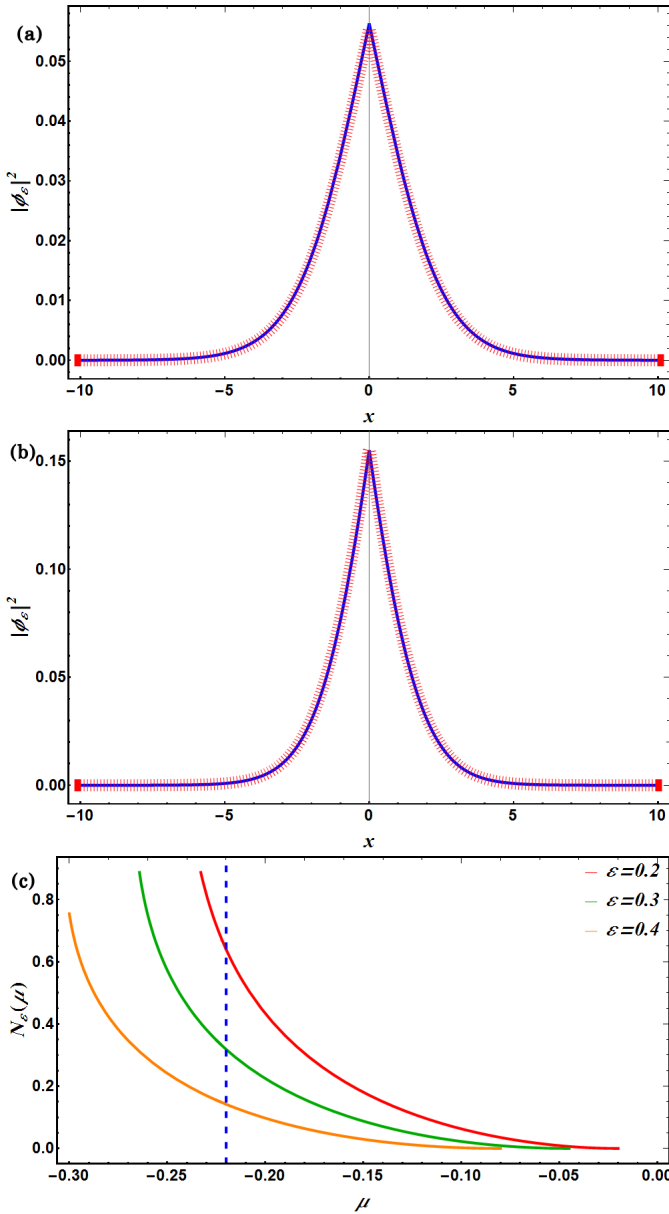


FIG. 3. (Color Online) Comparison between typical examples of analytical solutions (blue solid lines) given, respectively, by Eqs. (22), (23) and (30), (31) with their counterparts (red-bar lines), produced by the numerical solution of Eq. (6) [with the delta-function replaced by its Gaussian approximation (21)], is depicted in panels (a) and (b). The respective values of ε in (a) and (b) are 0.2 and 0.3. It is seen that the analytical and numerical solutions are indistinguishable. (c) The continuous dependence $N_\varepsilon(\mu)$, as produced by the analytical solutions given, severally, by Eqs. (22) and (23) at $\mu > -2/9$, and by Eqs. (30) and (31) at $\mu < -2/9$, for $\varepsilon = 0.2, 0.3$ and 0.4 (red, green, and orange lines, respectively). The vertical blue dashed line indicates the boundary between the two analytical solutions, $\mu = -2/9$. At $\mu < -2/9$, the curves are extended very close to the right edge of interval (32), $-\mu = 2/9 + \varepsilon^2/2$, beyond which solution (30) does not exist. Counterparts of these curves produced by the numerical solution (not shown here) are virtually identical to the analytical ones.

Exact solutions of Eq. (6) for QDs pinned to the delta-function potential well defined by Eq. (19), one can construct it as a direct extension of its free-space counterpart, given by Eq. (7), *viz.*,

$$\phi_\varepsilon(x, \mu) = -\frac{3\mu}{1 + \sqrt{1 + 9\mu/2} \cosh[\sqrt{-2\mu}(|x| + \xi)]}, \quad (22)$$

in the interval (8) of the values of μ , where the positive “lost length” (i.e., the shift of the maximum from its position in the absence of the attractive potential) is

$$2\xi = \sqrt{-\frac{2}{\mu}} \ln \left[\frac{\sqrt{\varepsilon^2 + (1 + 9\mu/2)(-2\mu - \varepsilon^2)} + \varepsilon}{\sqrt{1 + 9\mu/2}(\sqrt{-2\mu} - \varepsilon)} \right] \quad (23)$$

(this way of constructing solutions for QDs pinned to the delta-function potential was proposed in Ref. [41]). It is seen from Eq. (23) that the exact solutions for the pinned states exists in the following interval of values of the chemical potential,

$$\varepsilon^2/2 < -\mu < 2/9, \quad (24)$$

which is reduced in comparison to the bandgap mentioned in Eq. (8). Thus it follows from Eq. (24) that the pinned states of the QDs exist only if the delta-function pinning potential is not too strong, *viz.*,

$$\varepsilon < \varepsilon_{\max} = 2/3. \quad (25)$$

A majority of numerical results are reported below for $\varepsilon \equiv V_0 < 2/3$, i.e., condition (25) holds for them.

In the limit case of $\mu = -2/9$, the exact solution for the pinned QD, given by Eqs. (22) and (23) takes a simple but nontrivial form:

$$\phi_\varepsilon(x, \mu = -2/9) = \frac{2/3}{1 + \varepsilon(2/3 - \varepsilon)^{-1} \exp(2|x|/3)}. \quad (26)$$

Note that, while the exact solution in Eq. (7) with $\mu = -2/9$ degenerates into the CW state (15) with the divergent norm, solution (26) with the same μ remains a localized one, with a final norm [defined as per Eq. (9)]

$$N_\varepsilon(\mu = -2/9) = \frac{4}{3} \ln \left(\frac{2}{3\varepsilon} \right) - 2 \left(\frac{2}{3} - \varepsilon \right). \quad (27)$$

In the opposite limit corresponding to the left edge of interval (24),

$$\mu \rightarrow \mu_0 \equiv -\varepsilon^2/2, \quad (28)$$

the solution given by Eqs. (22) and (23) degenerates into

$$\phi_\varepsilon(x; \mu = -\varepsilon^2/2) = \mathcal{A} \exp(-\varepsilon|x|), \quad (29)$$

where \mathcal{A} is an arbitrary infinitesimal amplitude. This limit form of the solution is tantamount to the commonly known bound state maintained by the delta-function potential well in the framework of the linear Schrödinger equation.

A typical example of the exact solution produced by Eqs. (22) and (23) is displayed in Fig. 3(a), where it is compared to its counterpart produced by a numerical solution of Eq. (6) with the potential well taken as per Eqs. (18) and (20). It is seen that the analytical and numerical solutions are virtually identical ones.

The comparison of the value of the norm given by Eq. (27) and the infinitesimal norm at $\mu = -\varepsilon^2/2$ corresponding to Eq. (29) suggests that the dependence $N_\varepsilon(\mu)$ is monotonously decreasing. This feature, which is corroborated by Fig. 3(c), suggests that the family of pinned QDs are stable, according to the above-mentioned VK criterion (10). [45–47]. Their stability is indeed corroborated by direct simulations of Eq. (3) (not shown here in detail, as results of the simulations are straightforward).

In the presence of the attractive delta-functional potential, it is possible to find another exact solution for pinned QDs in the region of $\mu < -2/9$, where free-space solitons (7) *do not exist*. In the case when ε satisfies condition (25), this region extends the existence interval (8). The corresponding exact solution, which has no counterparts in the free space, is

$$\tilde{\phi}_\varepsilon(x) = -\frac{3\mu}{1 + \sqrt{-(1 + 9\mu/2)} \sinh[\sqrt{-2\mu}(|x| + \eta)]} \quad (30)$$

[cf. expression (7) for the solution constructed above], the positive “lost length” is

$$2\eta = \sqrt{-\frac{2}{\mu}} \ln \left[\frac{\sqrt{\varepsilon^2 - (1 + 9\mu/2)(\varepsilon^2 + 2\mu)} + \varepsilon}{\sqrt{-(1 + 9\mu/2)}(\sqrt{-2\mu} - \varepsilon)} \right], \quad (31)$$

cf. Eq. (23). Expression (30) is relevant if it yields real values of η . This condition holds in the following finite interval of values of the chemical potential,

$$2/9 \leq -\mu \leq 2/9 + \varepsilon^2/2. \quad (32)$$

It is a straightforward annex to interval (24) in which the above solution (22) exists. As well as the latter solution, the one given by Eqs. (30) and (31) satisfies the VK stability criterion (10), as shown in Fig. 3(c). Note that, in the limit of $\mu + 2/9 \rightarrow -0$, solution (30) takes the same form (26) to which the above solution (22) amounts at $\mu + 2/9 \rightarrow +0$, hence solution (30) provides smooth continuation of its counterpart (22) across the point of $\mu + 2/9 = 0$ [see an illustration in Fig. 3(c)].

The exact solution (30) can also be constructed in the region of

$$\varepsilon > 2/3, \quad (33)$$

i.e., outside of the region (25). In this case, expression (31) is replaced by

$$\eta = \frac{1}{\sqrt{-2\mu}} \ln \left[\frac{\varepsilon - \sqrt{\varepsilon^2 - (1 + 9\mu/2)(\varepsilon^2 + 2\mu)}}{\sqrt{-(1 + 9\mu/2)}(\sqrt{-2\mu} - \varepsilon)} \right], \quad (34)$$

and the solution exists in the same interval of the chemical potential as given by Eq. (32), while it has no counterpart at $-\mu < 2/9$. Indeed, in the limit of $\mu + 2/9 \rightarrow -0$

Eqs. (30) and (34) demonstrate that the solution degenerates into $\phi = 0$ [on the contrary to the nonzero solution (26), into which solution (22) carries over in the limit of $\mu + 2/9 \rightarrow +0$], thus providing the natural continuity with the absence of the pinned solution at $\mu > -2/9$ in the region (33). On the other hand, point (28), where solution (22) vanishes, as shown above [see Eq. (29)], is now an internal point of interval (32), due to condition (33). At this point, the present solution takes a relatively simple form,

$$\begin{aligned} \tilde{\phi}_\varepsilon(x; \mu = -\varepsilon^2/2) \\ = \frac{3\varepsilon^2/2}{1 + \sqrt{9\varepsilon^2/4 - 1} \sinh[\varepsilon|x| + (1/2) \ln(9\varepsilon^2/4 - 1)]}. \end{aligned} \quad (35)$$

The family of the exact solutions produced by Eqs. (30) and (34) also satisfies the VK criterion; in particular, the norm decreases from a finite value, corresponding to solution (35), at $\mu = -\varepsilon^2/2$ to $N = 0$ at $\mu = -2/9$. The compliance of the present family with the VK criterion implies its stability.

B. The Thomas-Fermi (TF) approximation for pinned state

A specific analytical approximation for solutions to Eq. (6) with the deep potential well (18), i.e., with large V_0 and $\mu < 0$, is provided by the TF approximation, which neglects the derivative (kinetic-energy) term:

$$\phi_{\text{TF}}(x) = \begin{cases} \frac{1}{2} + \sqrt{\frac{1}{4} - (V_0 - \mu)}, & \text{at } |x| < a, \\ \frac{1}{2} + \sqrt{\frac{1}{4} + \mu}, & \text{at } |x| > a \end{cases} \quad (36)$$

[in fact, the solution (36) at $|x| > a$ is relevant for the flat-top QD, with $\mu \approx -2/9$, the nearly constant solution around the potential well being close to the CW background (15)]. Then, for a small perturbation $\delta\phi$ added to $\phi_{\text{TF}}(x)$, the linearization of the nonlinear term in Eq. (6) produces, in the lowest approximation with respect to the fact that V_0 is a large parameter, an effective term in the GPE, $+3\varepsilon\delta(x) \cdot \delta\phi$, where ε is defined as per Eq. (20), and $\delta(x)$ is introduced in the same approximation as in Eq. (19). Then, the combination of this term and one corresponding to Eq. (19) gives rise to an effective *repulsive* potential,

$$f_{\text{effective}}(x) = +2\varepsilon\delta(x). \quad (37)$$

This crude analysis predicts, in a quantitative form, that the collision of a flat-top QD with the deep potential well may lead, instead of the naturally expected passage, to the counter-intuitive outcome in the form of *rebound*. This possibility is indeed demonstrated by numerical results reported below. It is relevant to mention that reflection of incident wave packets from a potential well is a well-known quantum effect, which was also elaborated in the framework of the MF theory [25, 26].

C. The interaction of the moving QD with a narrow potential barrier

As mentioned above, collisions of moving matter-wave packets with narrow potential barriers is a problem of high relevance for the design of soliton interferometers [35–39]. In the present context, treating the repulsive delta function potential (19) as a perturbation [51] makes it possible to predict the threshold value k_{thr} of velocity k [see Eq. (16)] which separates the rebound and passage of the incoming QD. In the adiabatic approximation, which neglects deformation of the QD under the action of the barrier, an effective potential of the interaction of the QD with the barrier can be found, in the adiabatic approximation (which neglects deformation of the QD due to its interaction with the local potential) as

$$U_{\text{eff}}(\Xi) = -\varepsilon \int_{-\infty}^{+\infty} \delta(x) |\psi(x - \Xi)|^2 dx$$

$$= -\frac{9\varepsilon\mu^2}{\left[1 + \sqrt{1 + 9\mu/2} \cosh(\sqrt{-2\mu}\Xi)\right]^2}, \quad (38)$$

where $\Xi(t)$ is the coordinate of the center of the moving QD. Obviously, the height of the effective potential barrier (38) is

$$U_{\text{max}} = \frac{9\varepsilon\mu^2}{\left(1 + \sqrt{1 + 9\mu/2}\right)^2}, \quad (39)$$

hence the comparison of this expression with the QD's kinetic energy (17) predicts the threshold value as

$$k_{\text{thr}}^2 = \frac{18\varepsilon\mu^2}{N(\mu) \left(1 + \sqrt{1 + 9\mu/2}\right)^2}, \quad (40)$$

where $N(\mu)$ is to be taken as per Eq. (9). The incident QD with $k < k_{\text{thr}}$ or $k > k_{\text{thr}}$ is expected, respectively, to bounce back or pass over the barrier.

In the limit case of flat-top QDs, which correspond to μ close to $-2/9$ [see Eq. (8)], Eqs. (39) and (40) take a simplified form:

$$U_{\text{max}} \approx \frac{4}{9}\varepsilon, \quad k_{\text{thr}}^2 \approx \frac{8\varepsilon}{9N}. \quad (41)$$

It may also be relevant to consider shuttle motion of the QD in a cavity formed by two narrow barriers, separated by a large distance L . The period of the motion with velocity k is $T = 2L/k$, hence the largest shuttle frequency which can be maintained by the cavity is $\omega_{\text{max}} = \pi k_{\text{thr}}/L$.

IV. NUMERICAL ANALYSIS

Following the analytical considerations presented in the previous section and compared to the numerical re-

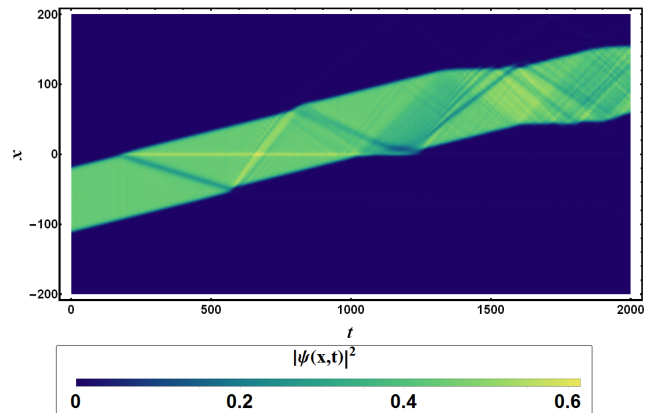


FIG. 4. (Color Online) The plot of the spatio-temporal evolution of the density, $|\psi(x,t)|^2$, presents an example of the full passage of the incident QD through the potential well, for $V_0 = 0.13$, $N = 40$ and $k = 0.1$.

sults in Fig. 3, in this section we aim to study the dynamics of QDs interacting with the potential well/barrier. To this end, simulations of Eq. (3) were performed by means of the split-step method based on the fast Fourier transform.

The numerical results are reported for the rectangular potential (18) with width $2a = 1$, which is small in comparison with other length scales, such as the width of the incident QDs (cf. Fig. 1), and justifies the comparison with approximation (19). In this case, Eq. (20) yields $\varepsilon = V_0$. We use zero boundary condition corresponding to an infinitely deep potential box occupying a broad spatial domain, $|x| < L = 200$. The initial wave function was taken as

$$\psi(x, t = 0) = \exp(ikx)\phi(x - x_{\text{init}}), \quad (42)$$

where $\phi(x)$ is the stationary solution (7) for the QD, k is the kick which sets the QD in motion, and x_{init} is its initial position.

A. Moving droplets

It is natural to expect that the travelling droplets colliding with the narrow potential well or barrier may demonstrate transmission or reflection, or even trapping, depending on the initial kick (k) in Eq. (42) and the strength of the potential. Splitting of the incident QD in transmitted, reflected, and trapped fragments may be expected too.

Norms of the transmitted, trapped, and reflected com-

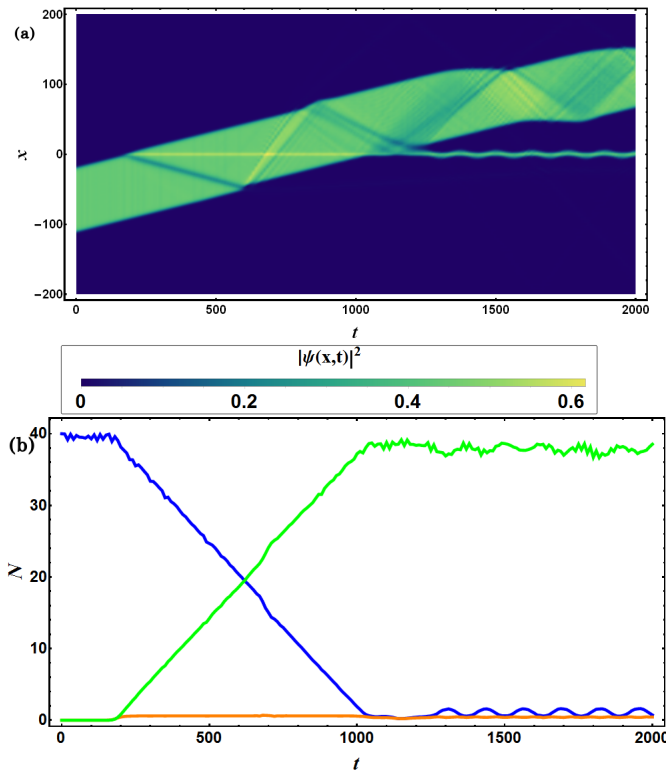


FIG. 5. (Color Online) (a) An example of the partial transmission of the incident QD through the potential well [as noted in Eq.(18)] with depth $V_0 = 0.14$. A very small share of the wave function is trapped in the well. (b) The temporal evolution of the norm for the transmitted (green solid line), trapped (orange solid line) and reflected (blue solid line) shares, defined as per Eqs. (43).

ponents of the wave function are defined as,

$$\begin{aligned}
 N_{\text{trans}} &= \int_a^L dx |\psi(x, t)|^2, \\
 N_{\text{trap}} &= \int_{-a}^{+a} dx |\psi(x, t)|^2, \\
 N_{\text{ref}} &= \int_{-L}^{-a} dx |\psi(x, t)|^2,
 \end{aligned} \quad (43)$$

which are subjected to the obvious constraint, $N_{\text{trans}} + N_{\text{trap}} + N_{\text{ref}} = N$.

First, we check effects of variation of the potential's strength for fixed k and N . The simulations started with the QD placed at $x_{\text{init}} = -65$ [see Eq. (42)] and moving with velocity $k > 0$ towards the local potential barrier/well defined by Eq. (18), with the width scaled to be $2a = 1$, as said above.

First, we present characteristic results obtained for the total norm $N = 40$ and velocity $k = 0.1$. We keep these values, unless mentioned otherwise. In particular, this relatively low collision velocity is appropriate for producing nontrivial results, while the fast moving QD simply passes the barrier/well, or elastically bounces back from

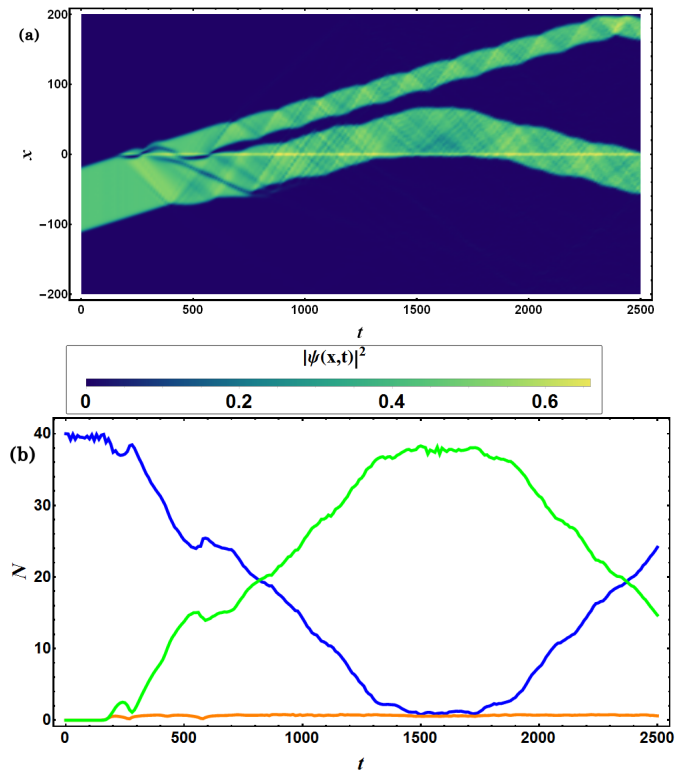


FIG. 6. (Color Online) (a) An example of the partial transmission and partial reflection of the incident QD colliding with the potential well, whose depth is $V_0 = 0.248$. (b) The temporal evolution of the transmitted (green solid line), trapped (orange solid line), and reflected (blue solid line) norms as defined in Eq. (43).

a very tall barrier. Conclusions valid for generic values of the N and k are presented below.

Figure 4 displays an example of the total transmission of the QD through the potential well (18) with depth $V_0 = 0.13$. Yellow lines in the density plot indicate excitations inside of the QD generated by the collision with the well (intrinsic excitation modes in quasi-1D QDs were studied in Ref. [20]). For values of the parameters corresponding to this figure, Eq. (41) yields $k_{\text{thr}} \approx 0.05$. The fact that this value is only half of the one used here, $k = 0.1$, immediately explains the total transmission observed in this case (the same argument explains the transmission in Fig. 5).

A trapped fraction of the wave field appears for a larger depth of the potential well. As an example, Fig. 5 shows the transmission with partial capture of the wave function at $V_0 = 0.14$. The small-amplitude narrow trapped component observed in this case is approximately described by solution (29) of the linearized equation. Further increase of V_0 causes partial reflection of the QD from the potential well, which is in qualitative agreement with the above prediction, see Eq. (37). The trapped share remains very small, as seen in Fig. 6 at $V_0 = 0.248$. The partial reflection may be interpreted

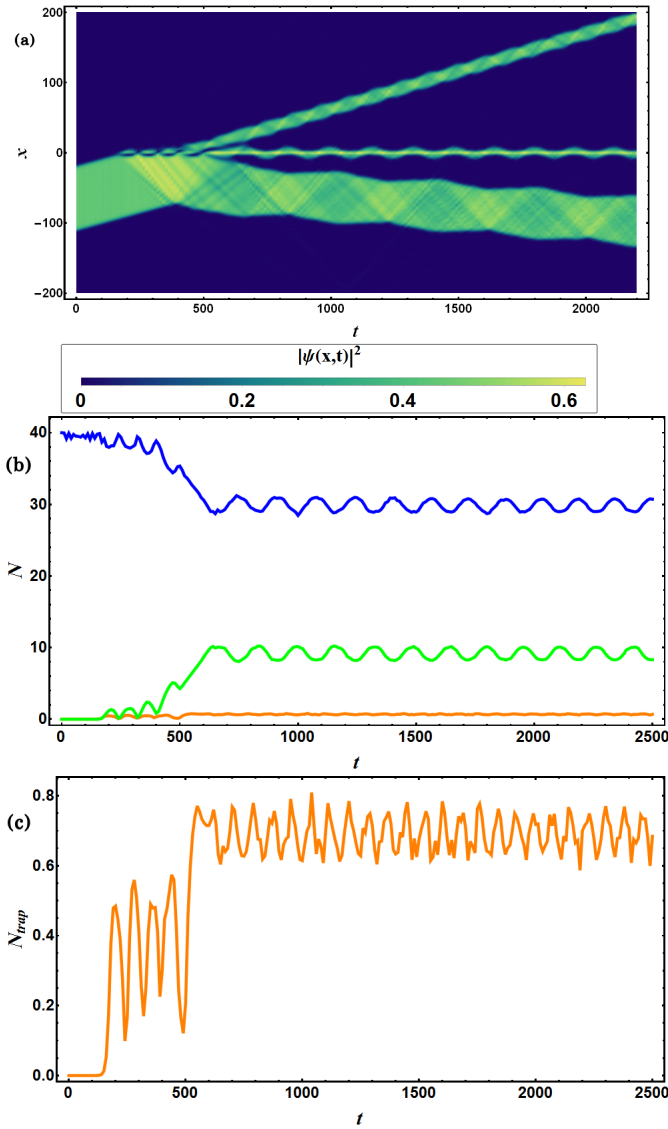


FIG. 7. (Color Online) (a) The splitting of the QD impinging onto potential well, with depth $V_0 = 0.3$, into the transmitted, trapped and reflected parts are depicted. (b) Description of the time evolution of the norm for transmitted (green solid line), trapped (orange solid line) and reflected waves (blue solid line). (c) The figure focuses on the evolution of the norm corresponding to the trapped wave. The complementary energy scenario is captured in Fig. 11

in a two-mode approximation [52], with the modes representing a small fraction of the droplet trapped in the well and the large moving one. When the two modes overlap, this may result in mutual repulsion when they are out of phase. Thus, when the QD is situated close to the narrow-potential's center, it may be reflected if the repulsion from the trapped mode overcomes the attraction force directly exerted by the potential.

The further increase of the depth of the potential well leads to a regime in which the incident QD splits in three different parts, *viz.*, the transmitted, reflected,

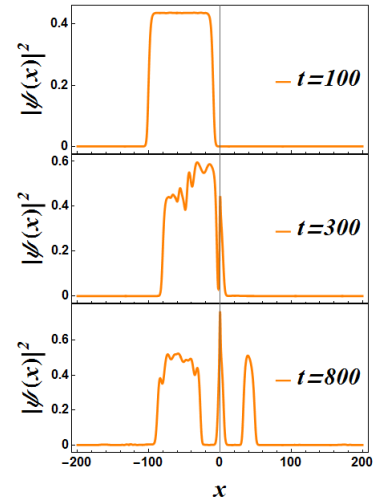


FIG. 8. (Color Online) Snapshots of the QD colliding with the potential well of depth $V_0 = 0.3$ at $t = 100$ (top panel), $t = 300$ (middle panel), $t = 800$ (bottom panel). Over the time the incident QD splits into a larger reflected part and a smaller transmitted one, along with a narrow trapped mode as described in the bottom panel.

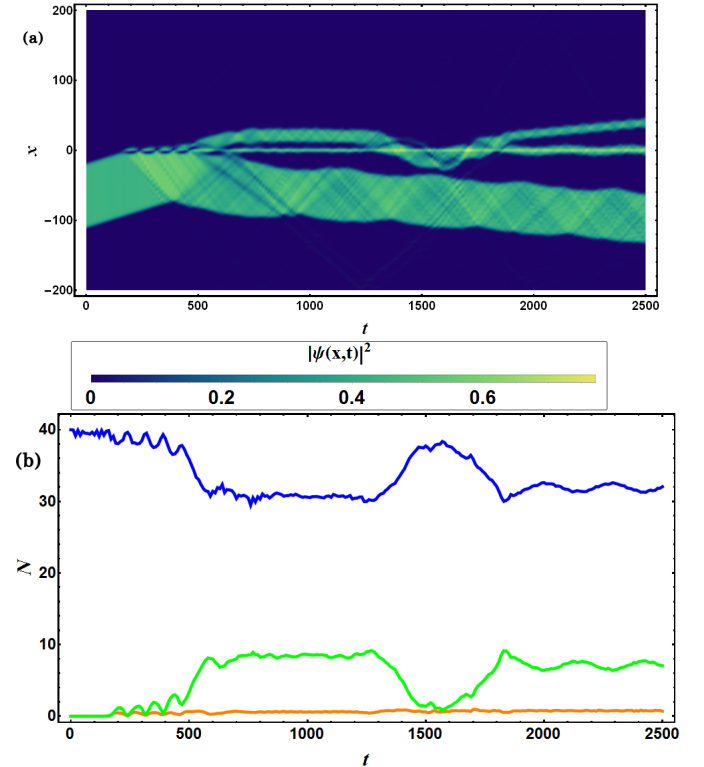


FIG. 9. (Color Online) (a) The partial reflection at $V_0 = 0.31$, with a very small packet trapped in the well. (b) The variation of the transmitted (green solid line), trapped (orange solid line) and reflected (blue solid line) norms are noted which clearly indicates a predominantly reflection of the waves.

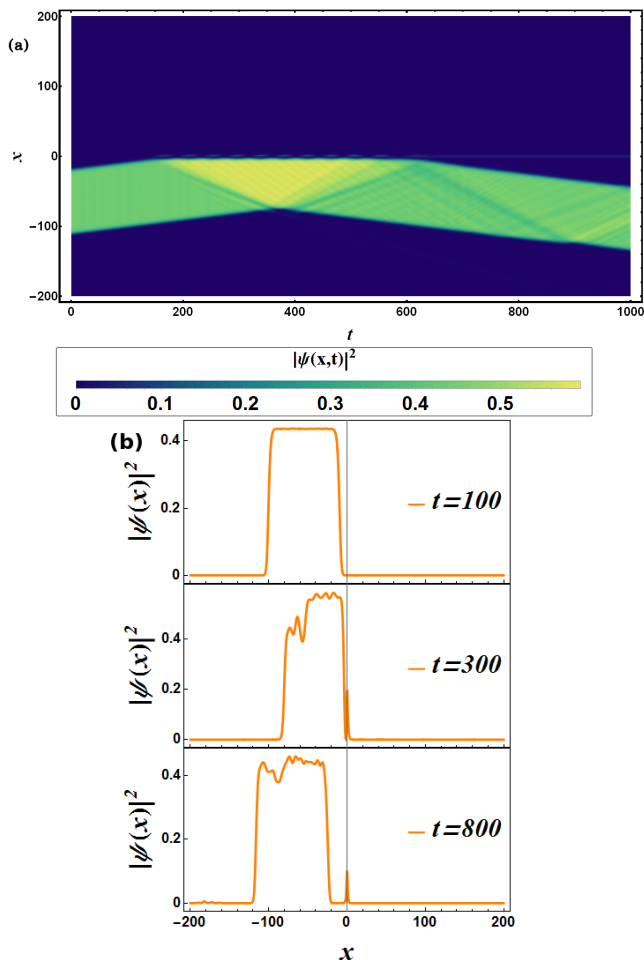


FIG. 10. (Color Online) (a) A reasonably deep potential well with depth $V_0 = 0.55$ leads to nearly total reflection of the QD. (b) Snapshots of the density profile at different times [$t = 100$ (top panel), $t = 500$ (middle panel) and $t = 800$ (bottom panel)] clearly substantiates the observation of (a). However, a very small fraction of trapped states can also be viewed from (a) and in the bottom panel of (b).

and (small) trapped wave packets. Figures 7 and 9 display examples of this outcome for depths $V_0 = 0.30$ and $V_0 = 0.31$, respectively. The former case is additionally illustrated in Fig. 8 by a set of snapshots of the density profiles. It is seen that all the three packets are produced by the collision is in excited states, and a small change of V_0 , from 0.30 to 0.31, leads to a conspicuous change of the dynamical picture. In terms of energy, these collisions are considered in the next subsection.

In accordance with the above qualitative analysis, based on the TF approximation and Eq. (37), nearly full reflection of the incident QD is observed at larger values of the well's depth V_0 , as illustrated in Figs. 10 for $V_0 = 0.55$. A very small trapped component is observed too, while transmission ceases to exist.

It is relevant to note that, besides the collision, splitting of the 1D QD into two or several fragments can also

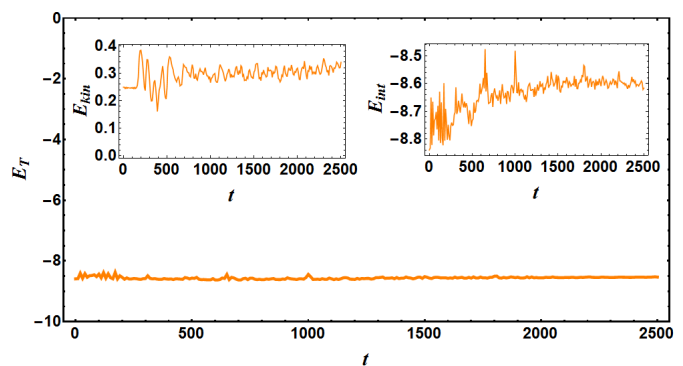


FIG. 11. (Color Online) Variation of the total energy over time. The total energy includes the contribution of the reflected, transmitted and trapped wave. The left inset describes the kinetic energy and trapped contribution while the right inset depicts the interaction energy evolution. It is clear from the picture that the total energy is heavily dominated by the interaction energy. The figure actually complements Fig. 7 in the context of energy calculation.

be caused by imprinting sufficiently small intrinsic excitation onto it [19]. Thus, flat-top QDs, even if they are stable solutions against small perturbations, are subject to internal fragility.

B. Analysis of energy in the trapping process

To consider the role of energy in the trapping dynamics driven by the attractive potential, we use Eq. (4) for the system's Hamiltonian, and address the case when the incident QD splits in three fragments, as shown in Figs. 7 (recall it corresponds to the collision of the QD with the potential well (18) of depth $V_0 = 0.3$). The results help to understand the situation in the general case as well.

In Fig. 11 variations of the kinetic and interaction energies are plotted for this case. The plots naturally demonstrate, for the flat-top QD, the domination of the negative potential energy, which saturates around a value -8.6 , over the kinetic energy, which takes values around 0.2. Further, Fig. 12 demonstrates that the kinetic energies of the transmitted and reflected wave packets are nearly equal, while their velocities and masses (norms) are widely different, as seen in Fig. 7. Simultaneously, the kinetic energy of the trapped packet oscillates around 0.006, indicating the presence of low-frequency excitations in it. On the other hand, the absolute values of the negative interaction (potential) energy in the reflected wave function is larger by a factor $\simeq 3$ than in the transmitted one, due to the obvious fact that the norm of the reflected packet is essentially larger in Fig. 7.

Due to the small values of the kinetic and interaction energies in the trapped wave, they are difficult to discern in Figs. 11 and 12. To make them visible, they are displayed in detail in Fig. 13. As said above, persistent

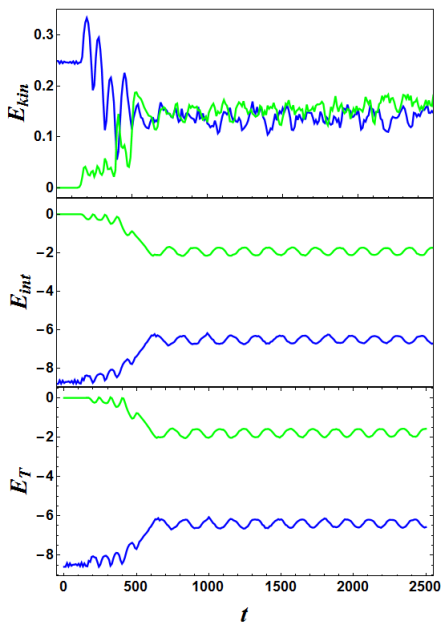


FIG. 12. (Color Online) The time evolution of the kinetic energy (top panel), interaction energy (middle panel) and total energy (bottom panel) for the reflected and transmitted components of the soliton. The green and blue lines describes the transmitted and reflected waves, respectively.

oscillations of the energies indicate that the trapped wave packet was created in the excited state. The ratio of the absolute values of the interaction and kinetic energies for this state is $\simeq 30$, which is comparable to the same ratios for the reflected and transmitted packets in Figs. 11 and 12.

C. Effects of variation of the norm (number of particles) and velocity on the QD scattering

As mentioned earlier, the collision of the QD with a sufficiently deep potential well tends to make the reflection (rather than the naively expected transmission) a dominant feature of the interaction [as predicted, in particular, by Eq. (37)]. For this reason, it is interesting to identify the largest well's depth, V_0 , which still admits the full transmission (passage) of the incident QD. Figure 14(a) presents a heatmap for such values of V_0 as a function of the droplet's norm (scaled number of particles), N , and speed, k . It is clearly seen that a maximum value of the so defined depth is achieved for moderate values of the norm, around $N \simeq 25$. This fact may be understood because the norm should be relatively large to consider the interaction with the potential well as a relatively weak perturbation, which cannot produce a conspicuous effect (such as the reflection) and, on the other hand, if the norm is too large, it will switch on the TF effect, which gives rise to the effective repulsive potential, as per Eq. (37). As for the effect of the velocity

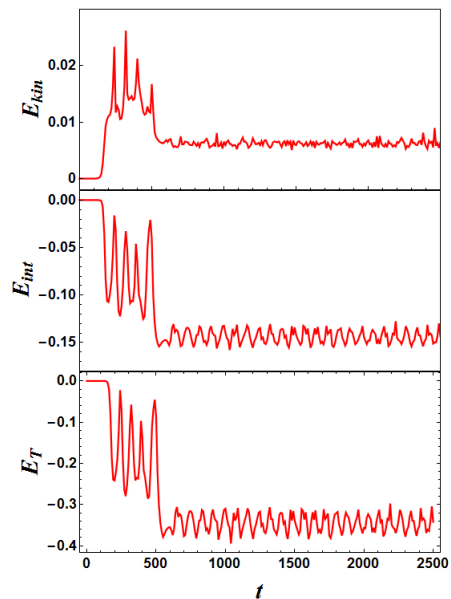


FIG. 13. (Color Online) The figure depicts the time evolution of the kinetic energy (top panel), interaction energy (middle panel) and the total energy (bottom panel) variation of the trapped state created by the collision of the incident QD with the narrow potential well. The current figure complements Fig. 7 in the context of energy calculation.

k , it may be explained, in a coarse approximation, by noting that, unless the collision is very slow, it excites the above-mentioned intrinsic oscillations in the trapped wave packet, which impedes the straightforward transmission. The above-mentioned counter-intuitive result, namely, the *full rebound* of the incident QD from the deep narrow potential well, deserves a detailed consideration too. The result is summarized in the Fig. 14(b), which presents, in the plane of (N, k) , a heatmap of the minimum (threshold) value of the well's depth, V_0 , above which the full rebound takes place. The asymptotic independence of the threshold on N is explained by the fact that the outcome of the collision of the incident flat-top QD with the narrow potential well is determined by the interaction of the well with the front (14) separating the zero and flat-top [near-CW, see Eq. (15)] levels of the density, irrespective of the width of the QD pattern.

Finally, we have performed the numerical analysis of the interaction of the incident QDs with the narrow barrier, which is represented by the narrow potential (18) with $V_0 < 0$. The results are summarized in Fig. 15, in which panel (a) and (b) display, respectively, the heatmaps, in the (N, k) plane, for the maximum value of V_0 which admits the full transmission of the incident QD, and the minimum (threshold) one above which the total rebound occurs. In the above-mentioned adiabatic approximation, which neglects deformation of the QD colliding with the potential barrier [51], both values of

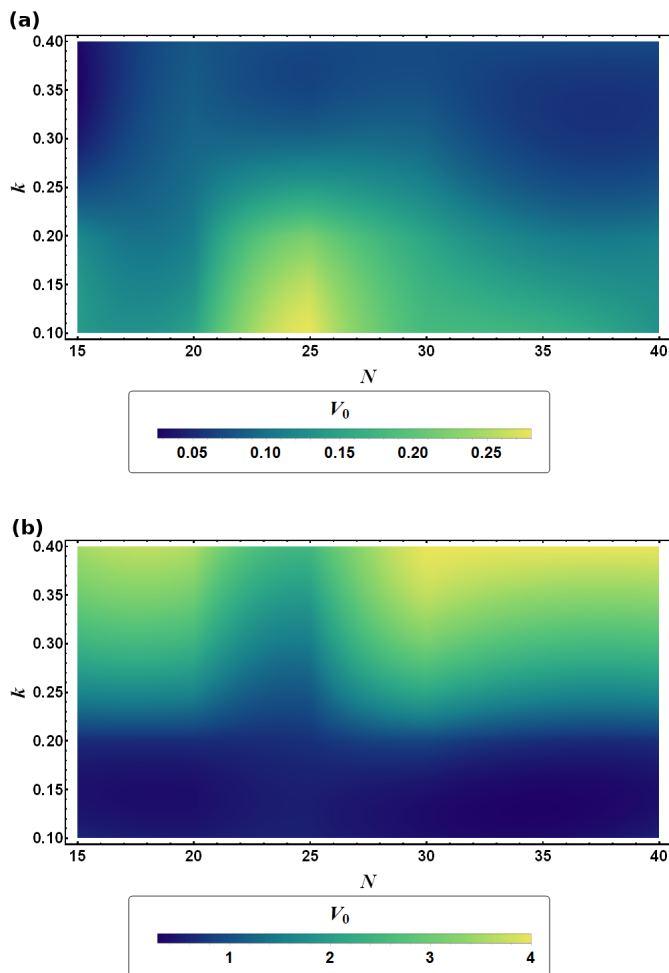


FIG. 14. (Color Online) (a) The pseudo-color map (*heatmap*) of the maximum value of the potential-well's depth V_0 which admits the full transmission (alias passage) of the incident QD, as a function of the QD's norm N and velocity k . (b) The heatmap of the minimum (threshold) value of V_0 which provides the counter-intuitive outcome of the collision, *viz.*, *full rebound* of the QD from the narrow potential well.

V_0 would be equal, given by Eq. (41) as

$$V_0 = 9Nk^2/8. \quad (44)$$

The strong difference between the top and bottom panels of Fig. 15 implies that the deformation, including fission of the incident QD into the transmitted and reflected fragments, is a conspicuous effect. Further, it is relevant to mention that, e.g., at $N = 20$ and $k = 0.25$ Fig. 15(b) produces $V_0 \simeq 2.5$, while Eq. (44) yields, for the same parameters, $V_0 \simeq 1.406$. The fact that the numerically found height of the potential barrier necessary for the full rebound is essentially larger than the prediction of the adiabatic approximation is explained by the occurrence of the tunneling effect, the suppression of which requires a taller barrier.

Nevertheless, Eqs. (40) and (41) make it possible to explain qualitative features observed in the bottom panel

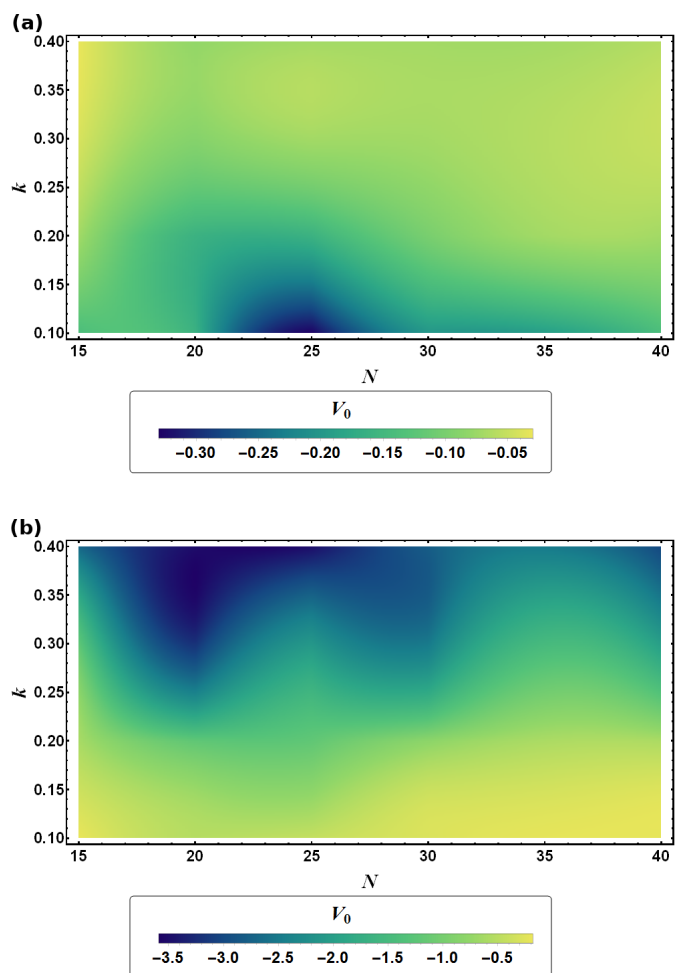


FIG. 15. (Color Online) (a) The maximum value of the height of the potential barrier, $-V_0$, which admits full transmission of the incident QD through the barrier, as a function of k and N . (b) The minimum value of $-V_0$, above which full reflection of the incident QD takes place, as a function of k and N .

of Fig. 15. In particular, this is the growth of the threshold value of V_0 with the increase of k at fixed N .

V. CONCLUSION

Using the known one-dimensional GPE (Gross-Pitaevskii equation) with the cubic self-repulsion and quadratic attraction induced by quantum fluctuations, we have studied in detail the static and dynamic solutions for QDs (quantum droplets) interacting with narrow potential wells and barriers. In the case of the potential represented by the delta-function potential, three different stable solutions for QDs pinned to the potential well are found in the exact form. The TF (Thomas-Fermi) approximation for the narrow rectangular well, and the adiabatic approximation for the collision of the QD with the potential barrier are elaborated too. Collisions of moving QDs with the well or barrier are systematically

studied by means of direct GPE simulations. The results are reported by means of diagrams in the plane of the QD's norm and velocity, which represent outcomes of the collisions, including the splitting of the incident QD into transmitted and reflected fragments, as well as a small trapped one. In particular, the counter-intuitive outcome in the form of the rebound of the QD from the potential well is identified and qualitatively explained. In the general case, the transmitted, reflected and trapped wave packets emerge in excited states, featuring intrinsic oscillations. Some peculiarities of the dynamical findings are explained by the analytical predictions.

As mentioned earlier, collisions of matter-wave solitons is a well-studied topic. Here, we have tried to extend the

systematic study for the interactions QDs with narrow potential wells and barriers. The theoretical results may be an incentive for experiments with QDs, and also propose new directions for the development of the matter-wave interferometry.

ACKNOWLEDGMENT

The work of B.A.M. was supported, in part, by the Israel Science Foundation through grant No. 1695/22. AK thanks Department of Science and Technology (DST), India for the support provided through the project number CRG/2019/000108.

-
- [1] T. D. Lee, K. Huang, and C. N. Yang, *Physical Review* **106**, 1135 (1957).
 - [2] D. Petrov, *Physical review letters* **115**, 155302 (2015).
 - [3] C. Cabrera, L. Tanzi, J. Sanz, B. Naylor, P. Thomas, P. Cheiney, and L. Tarruell, *Science* **359**, 301 (2018).
 - [4] P. Cheiney, C. Cabrera, J. Sanz, B. Naylor, L. Tanzi, and L. Tarruell, *Physical review letters* **120**, 135301 (2018).
 - [5] G. Semeghini, G. Ferioli, L. Masi, C. Mazzinghi, L. Wolswijk, F. Minardi, M. Modugno, G. Modugno, M. Inguscio, and M. Fattori, *Physical review letters* **120**, 235301 (2018).
 - [6] G. Ferioli, G. Semeghini, L. Masi, G. Giusti, G. Modugno, M. Inguscio, A. Gallemí, A. Recati, and M. Fattori, *Physical review letters* **122**, 090401 (2019).
 - [7] C. D'Errico, A. Burchianti, M. Prevedelli, L. Salasnich, F. Ancilotto, M. Modugno, F. Minardi, and C. Fort, *Phys. Rev. Res.* **1**, 033155 (2019).
 - [8] M. Schmitt, M. Wenzel, F. Böttcher, I. Ferrier-Barbut, and T. Pfau, *Nature* **539**, 259 (2016).
 - [9] L. Chomaz, S. Baier, D. Petter, M. Mark, F. Wächtler, L. Santos, and F. Ferlaino, *Physical Review X* **6**, 041039 (2016).
 - [10] Z.-H. Luo, W. Pang, B. Liu, Y.-Y. Li, and B. A. Malomed, *Frontiers of Physics* **16**, 1 (2021).
 - [11] A. Khan and A. Debnath, *Frontiers in Physics* , 534 (2022).
 - [12] D. Petrov and G. Astrakharchik, *Physical review letters* **117**, 100401 (2016).
 - [13] T. Ilg, J. Kumlin, L. Santos, D. S. Petrov, and H. P. Büchler, *Physical Review A* **98**, 051604 (2018).
 - [14] P. Zin, M. Pylak, and M. Gajda, *Physical Review A* **103**, 013312 (2021).
 - [15] M. Edmonds, T. Bland, and N. Parker, *Journal of Physics Communications* **4**, 125008 (2020).
 - [16] A. Debnath and A. Khan, *Ann. Phys. (Berlin)* **533**, 2000549 (2021).
 - [17] A. Debnath, A. Khan, and S. Basu, *Physics Letters A* **439**, 128137 (2022).
 - [18] E. Shamriz, Z. Chen, and B. A. Malomed, *Phys. Rev. A* **101**, 063628 (2020).
 - [19] G. Astrakharchik and B. A. Malomed, *Physical Review A* **98**, 013631 (2018).
 - [20] M. Tylutki, G. E. Astrakharchik, B. A. Malomed, and D. S. Petrov, *Physical Review A* **101**, 051601 (2020).
 - [21] N. Parker, A. Martin, S. Cornish, and C. Adams, *Journal of Physics B: Atomic, Molecular and Optical Physics* **41**, 045303 (2008).
 - [22] A. Marchant, T. Billam, M. Yu, A. Rakonjac, J. Helm, J. Polo, C. Weiss, S. Gardiner, and S. Cornish, *Physical Review A* **93**, 021604 (2016).
 - [23] H. Sakaguchi and M. Tamura, *Journal of the Physical Society of Japan* **73**, 503 (2004).
 - [24] R. H. Goodman, P. J. Holmes, and M. I. Weinstein, *Physica D: Nonlinear Phenomena* **192**, 215 (2004).
 - [25] C. Lee and J. Brand, *Europhysics Letters* **73**, 321 (2005).
 - [26] T. Ernst and J. Brand, *Physical Review A* **81**, 033614 (2010).
 - [27] L. D. Carr, R. R. Miller, D. R. Bolton, and S. A. Strong, *Physical Review A* **86**, 023621 (2012).
 - [28] C.-H. Wang, T.-M. Hong, R.-K. Lee, and D.-W. Wang, *Optics Express* **20**, 22675 (2012).
 - [29] A. Harel and B. A. Malomed, *Physical Review A* **89**, 043809 (2014).
 - [30] L. Al Sakkaf and U. Al Khawaja, *Phys. Rev. E* **107**, 014202 (2023).
 - [31] J. L. Helm, T. P. Billam, and S. A. Gardiner, *Physical Review A* **85**, 053621 (2012).
 - [32] B. Gertjerenken, T. P. Billam, L. Khaykovich, and C. Weiss, *Physical Review A* **86**, 033608 (2012).
 - [33] S.-C. Li and F.-Q. Dou, *Europhysics Letters* **111**, 30005 (2015).
 - [34] C. L. Grimshaw, S. A. Gardiner, and B. A. Malomed, *Physical Review A* **101**, 043623 (2020).
 - [35] A. Martin and J. Ruostekoski, *New Journal of physics* **14**, 043040 (2012).
 - [36] J. Polo and V. Ahufinger, *Physical Review A* **88**, 053628 (2013).
 - [37] J. Helm, S. Rooney, C. Weiss, and S. Gardiner, *Physical Review A* **89**, 033610 (2014).
 - [38] O. J. Wales, A. Rakonjac, T. P. Billam, J. L. Helm, S. A. Gardiner, and S. L. Cornish, *Communications Physics* **3**, 51 (2020).
 - [39] C. L. Grimshaw, T. P. Billam, and S. A. Gardiner, *Physical Review Letters* **129**, 040401 (2022).
 - [40] H. Sakaguchi and B. A. Malomed, *New Journal of Physics* **18**, 025020 (2016).
 - [41] F. K. Abdullaev and R. Galimzyanov, *Journal of Physics B: Atomic, Molecular and Optical Physics* **53**, 165301

- (2020).
- [42] G. Bighin, A. Burchianti, F. Minardi, and T. Macrì, *Phys. Rev. A* **106**, 023301 (2022).
- [43] S. Sinha, S. Biswas, L. Santos, and S. Sinha, arXiv preprint arXiv:2304.04261 (2023).
- [44] M. Pylak, F. Gampel, M. Płodzień, and M. Gajda, *Phys. Rev. Res.* **4**, 013168 (2022).
- [45] N. Vakhitov and A. Kolokolov, *Izv Vyssh Uchebn Zaved Radiofiz* **16**, 1020 (1973).
- [46] L. Bergé, *Physics reports* **303**, 259 (1998).
- [47] G. Fibich, *The nonlinear Schrödinger equation: singular solutions and optical collapse*, Vol. 192 (Springer, 2015).
- [48] D. J. Korteweg and G. De Vries, *The London, Edinburgh, and Dublin Philosophical Magazine and Journal of Science* **39**, 422 (1895).
- [49] S. Novikov, S. V. Manakov, L. P. Pitaevskii, and V. E. Zakharov, *Theory of solitons: the inverse scattering method* (Springer Science & Business Media, 1984).
- [50] L. Wang, B. A. Malomed, and Z. Yan, *Physical Review E* **99**, 052206 (2019).
- [51] Y. S. Kivshar and B. A. Malomed, *Reviews of Modern Physics* **61**, 763 (1989).
- [52] T. Ernst and J. Brand, *Phys. Rev. A* **81**, 033614 (2010).